AGU PUBLICATIONS

Geophysical Research Letters

RESEARCH LETTER
10.1002/2016GL071719

Key Points:
- The pH seasonality is reproduced using sensitivity factors and dissolved inorganic carbon (DIC), temperature, and alkalinity (TA) seasonalities
- Variations in DIC and temperature are the main drivers of pH seasonality and act in opposite directions, with a modulating role for TA
- Temperature and DIC are the principal drivers of pH variability at low to middle and high latitudes, respectively

Supporting Information:
- Supporting Information S1

Correspondence to:
M. Hagens,
m.hagens@uu.nl

Citation:
Hagens, M., and J. J. Middelburg (2016), Attributing seasonal pH variability in surface ocean waters to governing factors, *Geophys. Res. Lett.*, *43*, 12,528–12,537, doi:10.1002/2016GL071719.

Received 27 OCT 2016
Accepted 5 DEC 2016
Accepted article online 8 DEC 2016
Published online 27 DEC 2016

Attributing seasonal pH variability in surface ocean waters to governing factors

M. Hagens[1] **and J. J. Middelburg**[1]

[1]Department of Earth Sciences - Geochemistry, Utrecht University, Utrecht, Netherlands

Abstract On-going ocean acidification and increasing availability of high-frequency pH data have stimulated interest to understand seasonal pH dynamics in surface waters. Here we show that it is possible to accurately reproduce observed pH values by combining seasonal changes in temperature (*T*), dissolved inorganic carbon (DIC), and total alkalinity (TA) from three time series stations with novel pH sensitivity factors. Moreover, we quantify the separate contributions of *T*, DIC, and TA changes to winter-to-summertime differences in pH, which are in the ranges of −0.0334 to −0.1237, 0.0178 to 0.1169, and −0.0063 to 0.0234, respectively. The effects of DIC and temperature are therefore largely compensatory, and are slightly tempered by changes in TA. Whereas temperature principally drives pH seasonality in low-latitude to midlatitude systems, winter-to-summer DIC changes are most important at high latitudes. This work highlights the potential of pH sensitivity factors as a tool for quantifying the driving mechanisms behind pH changes.

1. Introduction

The invasion of anthropogenic carbon dioxide (CO_2) from the atmosphere into the ocean has not only attenuated accumulation of CO_2 in the atmosphere and thus global warming but also caused ocean acidification [*Kleypas et al*., 1999]. Long-term observations show that ocean pH declines on average about 0.002 units per year in open ocean settings [*Bates et al*., 2014; *Lauvset et al*., 2015; *Ríos et al*., 2015], consistent with theoretical calculations. Model simulations indicate that ocean pH has already declined by 0.1 units since the start of the industrial time and that surface water pH will decline further by 0.3 to 0.5 units depending on location and emission scenarios [*Orr*, 2011; *Bopp et al*., 2013]. This may have major consequences for multiple biological processes, including calcification, primary production, and nitrogen fixation [*Gattuso et al*., 2014]. Superimposed on this long-term declining pH trend are diurnal, seasonal, and interannual changes [*Wootton and Pfister*, 2012; *Kapsenberg and Hofmann*, 2016; *Sutton et al*., 2016]. The magnitudes of these shorter-term pH fluctuations are similar or larger than the pH decline projected for the end of this century [*Wootton et al*., 2008; *Provoost et al*., 2010; *Hofmann et al*., 2011]. It is therefore essential to identify the drivers of these pH fluctuations and to improve our capabilities to predict ocean pH variability.

Wootton et al. [2008] and *Wootton and Pfister* [2012] fit a semimechanistic model to high-frequency data using nonlinear regression to identify the drivers of ocean pH change in coastal waters of Washington State, USA. Temperature (*T*), salinity (*S*), total alkalinity (TA), upwelling, and biological processes were identified to contribute significantly to variance in pH. *Flecha et al*. [2015] reported high-frequency pH records from the Strait of Gibraltar and attributed pH variability to different water mass contributions. *Kapsenberg and Hofmann* [2016] presented high-resolution ocean pH time series and found that temperature, upwelling/mixing, and biological processes explained most of the pH variability along the northern Channel Islands, California, USA. These observational studies provide a first step toward understanding pH dynamics but ignore chemical reactions buffering changes in pH. The amplitude of variability in pH and other carbonate system parameters depends not only on the magnitude of the drivers but also on the sensitivity of the system to changes in ocean chemistry, biology, and physics [*Frankignoulle*, 1994; *Sarmiento and Gruber*, 2006; *Takahashi et al*., 2014]. Low-latitudinal, warm waters, for example, are relatively insensitive [*Orr*, 2011], whereas polar waters have a naturally low buffering capacity and therefore display larger carbonate system variability [*Fabry et al*., 2009; *Shadwick et al*., 2013]. A more mechanistic approach involving knowledge on the drivers of changes as well as the sensitivity of the system is the next step toward improved understanding of ocean pH variability.

Several studies have quantified the drivers of seasonal and/or interannual variability in mixed layer dissolved inorganic carbon (DIC) using a diagnostic box model based on time series data [*Gruber et al*., 1998, 2002; *Keeling et al*., 2004; *Shadwick et al*., 2011]. *Takahashi et al*. [1993] derived an explicit relationship between the partial pressure of CO_2 (pCO_2) and temperature. This equation allows the partitioning of the seasonal variability in pCO_2 due to temperature and changes in chemistry [*Keeling*, 1993; *Takahashi et al*., 2002; *Riebesell et al*., 2009]. *Sarmiento and Gruber* [2006] extended this approach and presented pCO_2 sensitivities for *T*, *S*, DIC, and TA, which they used to partition the seasonal pCO_2 record into temperature and DIC components. Recently, *Takahashi et al*. [2014] presented numerically derived sensitivities for pCO_2, pH, and the saturation states of calcite (Ω_{cal}) and aragonite (Ω_{ara}) and used these to calculate seasonal amplitudes of pCO_2, pH, and these saturation states at five stations.

Inspired by *Frankignoulle* [1994], *Hagens and Middelburg* [2016] derived a generic set of explicit equations describing the sensitivity of pH to changes in ocean chemistry. In this study we use these sensitivities to calculate seasonal changes in pH resulting from changes in *T*, *S*, TA, and DIC, as well as other acid-base systems, at three ocean time series stations: DYnamique des Flux Atmosphériques en MEDiterranée (DYFAMED) in the Mediterranean Sea, A Long-Term Oligotrophic Habitat Assessment (ALOHA) in the North Pacific gyre, and Iceland Sea in the North Atlantic. We aim to show that seasonality in pH can be predicted from seasonal variability in TA, DIC, and temperature, and to quantify the driving factors of the seasonal variations in pH in oceanic systems.

2. Methods

2.1. Time Series Station Data

Three time series stations with seasonal resolution were chosen (see supporting information for details): (1) the highly saline Mediterranean Sea (DYFAMED; located in the Ligurian Sea [*Pasqueron de Fommervault et al*., 2015; *Coppola et al*., 2016]); (2) the oligotrophic Pacific open ocean (Station ALOHA [*Dore et al*., 2003, 2009]), and (3) the high-latitude Iceland Sea [*Olafsson et al*., 2010; *Olafsson*, 2014]. From all stations, we only used data between 0 and 10 m water depth and selected those cruises where at least two carbonate system parameters were measured. In case of carbonate system overdetermination, we used DIC and TA. If a nutrient had not been measured, we used the global climatological surface-ocean average for the year 2000.

To obtain a seasonal cycle from the DYFAMED, ALOHA, and Iceland Sea data sets, we applied the method of *Gruber et al*. [1998, 2002] and *Keeling et al*. [2004]. This method involves removing a statistically significant ($P < 0.05$) linear trend from the data (this step was discarded for the DYFAMED data set, where significant trends could not be obtained for most parameters) followed by combining the detrended data into a composite year, thereby neglecting interannual variations. This composite year thus represents a climatological average for the period that the data spans [*Gruber et al*., 1998]. Then, we used a least squares method [*Bates and Watts*, 1988] to fit the following harmonic function to each parameter of the composite year separately:

$$H = \sum_{k=1}^{m} \left[a_k \sin\left(\frac{2\pi k t}{Y}\right) + b_k \cos\left(\frac{2\pi k t}{Y}\right) \right] + H_0 \quad (1)$$

Here *H* is the fitted parameter value, *t* is Julian day, and *Y* is the length of 1 year, i.e., 365 days. Following *Keeling et al*. [2004] and *Gruber et al*. [2002], we applied equation (1) as a three-harmonic function ($m = 3$) with periods of 12 ($k = 1$), 6 ($k = 2$), and 4 ($k = 3$) months. The coefficients *a* and *b* and corresponding P values for each parameter, as well as H_0, which represents the annual mean of that parameter, are presented in the supporting information. In further calculations, we only included the coefficients that produced a statistically significant fit (i.e., $P < 0.05$, calculated using the *stats* package in R [*R Core Team*, 2016]).

2.2. Modeling pH

Two methods were applied to reproduce composite year pH. First, observed pH values were fitted to the harmonic function (equation (1)) in a similar way as the other parameters (pH_{fit}). Second, pH was predicted

(pH_{pred}) using equation (2), which is effectively the total derivative of pH as a function of *T*, *S*, DIC, TA, total borate (TotB), total sulfate ($TotSO_4$), total fluoride (TotF), and nutrients:

$$\begin{aligned} &\mathrm{pH}_{pred}\left(T, S, \mathrm{DIC}, \mathrm{TA}, TotB, \mathrm{TotSO_4}, \mathrm{TotF}, \sum_{i=1}^{j}\mathrm{nutrient}\right) = \overline{\mathrm{pH}} \\ &+\frac{\partial \mathrm{pH}}{\partial T}\left(\overline{T} - T\right) + \frac{\partial \mathrm{pH}}{\partial S}\left(\overline{S} - S\right) + \frac{\partial \mathrm{pH}}{\partial \mathrm{DIC}}\left(\overline{DIC} - \mathrm{DIC}\right) + \frac{\partial \mathrm{pH}}{\partial \mathrm{TA}}\left(\overline{\mathrm{TA}} - \mathrm{TA}\right) \\ &+\frac{\partial \mathrm{pH}}{\partial \mathrm{TotB}}\left(\overline{\mathrm{TotB}} - \mathrm{TotB}\right) + \frac{\partial \mathrm{pH}}{\partial \mathrm{TotF}}\left(\overline{\mathrm{TotF}} - \mathrm{TotF}\right) \\ &+\frac{\partial \mathrm{pH}}{\partial \mathrm{TotSO_4}}\left(\overline{\mathrm{TotSO_4}} - \mathrm{TotSO_4}\right) + \sum_{i=1}^{j}\frac{\partial \mathrm{pH}}{\partial \mathrm{nutrient}}\left(\overline{\mathrm{nutrient}} - \mathrm{nutrient}\right) \end{aligned} \quad (2)$$

Here the parameters with overbars represent the fitted annual means (H_0), with the exception of $\overline{pH}$, which is calculated using the H_0 values of the other parameters. The partial derivatives, except those with respect to *T* and *S*, represent the sensitivities analytically calculated following *Hagens and Middelburg* [2016]. These factors, which describe the response of pH to a change in TA or the total concentration of an acid-base species, are an extension of the work by *Frankignoulle* [1994] and *Egleston et al*. [2010] and based on the definition of TA given by *Dickson* [1981] but include the acid-base systems mentioned by *Soetaert et al*. [2007]. The sensitivities of pH with respect to *T* and *S* were numerically determined following *Hofmann et al*. [2009]. To determine the principal drivers of pH seasonality, we varied each of the parameters in equation (2) separately, thereby keeping the other parameters at their fitted annual mean values.

All calculations were done with the R package *AquaEnv* [*Hofmann et al*., 2010] at in situ temperature and using the free pH scale. Where applicable, nutrient concentrations were converted from $\mu mol\,L^{-1}$ to $\mu mol\,kg^{-1}$. The *Lueker et al*. [2000] carbonate system equilibrium constants were used following best practices [*Dickson et al*., 2007]. *AquaEnv* defaults were used for the CO_2 solubility constant and the other acid-base dissociation constants.

3. Results

3.1. Seasonality in the Factors Driving pH

At DYFAMED the seasonal cycle of DIC, with 12, 6, and 4 month periodicities, peaks at 2285 $\mu mol\,kg^{-1}$ in late February. This is followed by a sharp decline until mid-June and a gradual decrease to a minimum of 2226 $\mu mol\,kg^{-1}$ in late August, after which it increases again (Figure 1a). Temperature decreases until mid-February (13.2°C), increases from mid-February to mid-August (23.3°C), and declines afterward. Thus, temperature and DIC changes are in opposite directions, with temperature extremes preceding those of DIC by a few weeks (Figures 1a and 1d). Seasonality in TA is limited compared to both DIC and temperature; has 12, 6 and 4 month periodicities (Figure 1g); and shows a minimum of 2552 $\mu mol\,kg^{-1}$ in early January and maxima of 2572 $\mu mol\,kg^{-1}$ in mid-March and mid-October.

At Station ALOHA DIC initially increases to a maximum of 1965 $\mu mol\,kg^{-1}$ in early March, followed by a decrease to 1952 $\mu mol\,kg^{-1}$ in early September, and increases thereafter (Figure 1b). DIC seasonality at ALOHA is less constrained than at the DYFAMED or Iceland Sea stations (Figures 1a–1c) and only shows a 12 month signal, whereas both DIC and temperature at the DYFAMED station have minor shorter-term signals superimposed on the 12 month periodicity (supporting information). At Station ALOHA temperature (Figure 1e) declines until early March (23.3°C), increases until late September (26.3°C), and decreases again thereafter. Its seasonal pattern generally opposes that of DIC and has similar periodicities as temperature at DYFAMED. Similar to DIC, intraannual variability in TA (Figure 1h) is not well constrained and only shows a 12 month periodicity, varying between 2300 $\mu mol\,kg^{-1}$ in early January and 2293 $\mu mol\,kg^{-1}$ in early July.

At the Iceland Sea site DIC increases to a maximum of 2142 $\mu mol\,kg^{-1}$ in mid-March and then declines to a mid-September minimum (2058 $\mu mol\,kg^{-1}$). The temporal pattern is, however, more complex with additional 6 and 4 month periodicities, resulting in a minor DIC increase in May and a small drawdown in December (Figure 1c). Temperature rises from a minimum of −0.85°C in mid-March to a maximum of 7.5°C in late August. Its seasonal cycle has 12, 6, and 4 month periodicities, and the initial increase is relatively slow until late May, whereas the initial decline from late August onward is comparably fast (Figure 1f). DIC and

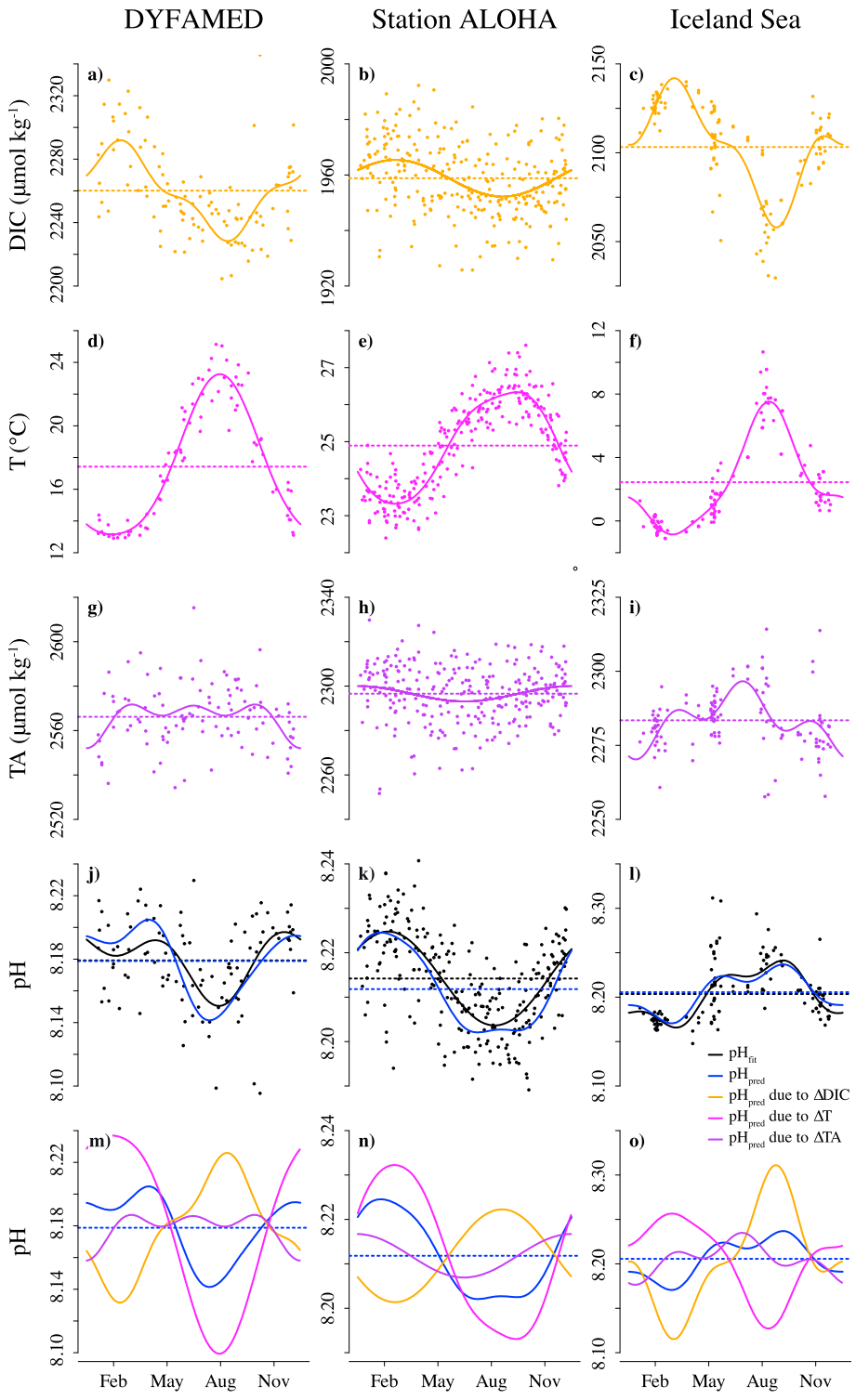

Figure 1. Composite year data and corresponding harmonic functions (fitted using equation (1)) for (a–c) DIC (µmol kg^{-1}), (d–f) temperature (°C), (g–i) TA (µmol kg^{-1}), and (j–l) pH for the DYFAMED, ALOHA, and Iceland Sea stations. (m–o) The changes in pH_{pred} over the year resulting from the isolated changes in DIC, temperature, and TA, which are calculated using equation (2), and the sum of all isolated changes (i.e. including the minor contributions from variations in salinity and nutrient concentrations). For comparative purposes, this sum (pH_{pred}) is also added to the plots of the observed pH data and pH_{fit} (Figures 1j–1l).

temperature generally show opposing behavior, but due to the different contributions of the various periodicities, the temperature maximum precedes the DIC minimum by a few weeks. Seasonality in TA is most pronounced at the Iceland Sea site, displaying 12 and 4 month periodicities (Figure 1i), with a maximum of 2297 μmol kg^{-1} in mid-July and a minimum of 2270 μmol kg^{-1} in mid-January.

The peak-to-peak amplitudes of the harmonic fits for DIC, temperature, and TA at the Iceland Sea site are 84 μmol kg^{-1}, 8.4°C, and 26 μmol kg^{-1}, respectively. At station DYFAMED annual maximum and minimum values differ by 59 μmol kg^{-1} for DIC, 10.1°C for temperature, and 20 μmol kg^{-1} for TA, whereas at Station ALOHA the respective intraannual variabilities are 13 μmol kg^{-1}, 3.0°C, and 6.9 μmol kg^{-1}.

3.2. Seasonality in pH

At all stations, seasonality in pH is reproduced, whether estimated with a harmonic fitting function (pH_{fit} (Equation (1), black line) or predicted using Equation (2) (pH_{pred}, blue line). pH_{pred} values were calculated using the seasonality of all factors affecting pH, i.e., also including salinity and nutrients, which only have a minor effect on pH variability at these sites (not shown). At DYFAMED intraannual variability of pH_{fit} (Figure 1j; black line) is driven by the 12 and 6 month signals, with a peak-to-peak amplitude of 0.0467. The minimum in pH_{fit} occurs in mid-August, whereas the maximum is found in early December. Intraannual variability in pH_{pred} occurs on similar timescales, its minimum and maximum closely resemble those of pH_{fit}, and the difference between its extremes is somewhat higher (0.0635).

The composite year of pH_{fit} at station ALOHA reveals a 12 month periodicity (Figure 1k) with a peak-to-peak amplitude of 0.0212. pH_{fit} increases until late February, and subsequently declines until late August, before increasing again. In contrast, pH_{pred} shows a global minimum in late July and a global maximum in early February, but in addition local extremes in early September and late October are found. The peak-to-peak amplitude of pH_{pred} is, however, almost identical to that of pH_{fit} (0.0208).

At the Iceland Sea site, processes acting on multiple timescales influence pH_{fit} (Figure 1l), but the 12 month signal dominates variability. Consequently, there is a 6 month difference between the maximum (8.241, in mid-September) and minimum pH_{fit} (8.166, in mid-March). The calculated pH_{pred} values closely match the pattern of pH_{fit}, although the minimum pH_{pred} slightly precedes the minimum in pH_{fit}. The amplitudes of fitted (0.0757) and predicted (0.0664) pH values are similar at the Iceland Sea station.

There is therefore a very good agreement between fitted and predicted pH for the DYFAMED, ALOHA, and Iceland Sea stations, with maximum absolute differences between pH_{pred} and pH_{fit} of 0.0167, 0.00554, and 0.0114, respectively.

3.3. Quantifying the Drivers of Seasonal pH Variability

Seasonal pH dynamics can be well predicted using DIC, TA, and temperature as governing factors. Moreover, the effects of DIC and temperature are largely compensatory (Figures 1m–1o). At DYFAMED, pH_{pred} in January is somewhat above its annual average and initially declines slightly (Figure 1m) due to a DIC increase that has a stronger effect than the minor temperature decrease and TA increase. From late February onward, temperature increases, causing a lowering in pH, but the drawdown of DIC is stronger, resulting in a net increase in pH_{pred}. This situation lasts until late April, when the decrease in DIC slows down, thus lowering pH_{pred}. Between late April and late November, the effect of temperature dominates over the DIC signal, whereas variations in TA hardly have an impact: pH_{pred} increases until mid-August and declines afterward, matching the trend in temperature. From late November onward, the effect of the decline in temperature is compensated for by the increase in DIC and decrease in TA, leading to only minor changes in pH_{pred}. The peak-to-peak amplitudes of the DIC-, temperature-, and TA-induced pH changes are 0.0945, 0.1357, and 0.0288, respectively.

At Station ALOHA, pH_{pred} dynamics are mainly driven by temperature but attenuated by the changes in DIC that always have an opposite effect on pH_{pred} (Figure 1n). The extent to which this dampening occurs varies throughout the year: this is due to the 6 month periodicity that is absent for DIC but present for temperature. The effect of TA variability on pH is minor; however, the increase in TA from early July onward brings forward the pH_{pred} minimum and contributes to the creation of its local extremes. Similar to at DYFAMED, the peak-to-peak difference in pH due to DIC (0.0210) is smaller than that due to temperature (0.0392), whereas the maximum pH difference due to TA changes is only 0.00980.

Seasonal pH variability at the Iceland Sea station is more evenly governed by temperature, DIC, and TA and is therefore more complicated to disentangle (Figure 1o). Furthermore, the harmonic fitting procedure reveals that variability in these parameters occurs on multiple timescales (Figures 1c, 1f, and 1i). In January, pH_{pred} is somewhat lower than average, because of a lower-than-average TA, which acts to decrease pH, and a slightly lower-than-average temperature, attenuating this pH decrease. Subsequently, pH_{pred} declines due to a strong increase in DIC, which is only partly compensated for by the increase in TA and a decrease in temperature. Between early March and the end of May, pH_{pred} increases due to a decrease in DIC, again dampened by the increasing temperature. The combined effect of all three drivers is responsible for the complex pH dynamics between June and September. From mid-September to mid-November, pH_{pred} decreases, primarily due to the increase in DIC, but again attenuated by the decrease in temperature and remains low from mid-November onward due to the counterbalancing decreases in both TA and DIC. In contrast to the DYFAMED and ALOHA stations, the peak-to-peak difference in pH of the DIC-driven change is higher (0.1958) than that of temperature signal (0.1296). Variability in TA leads to the smallest maximum pH change (0.0585).

4. Discussion

4.1. Seasonal Variability at the DYFAMED Station

Previous studies at the DYFAMED station focusing on pCO_2 have shown that its seasonal variability, which has an amplitude of 120–200 ppmv, is mainly driven by temperature but dampened by net community production (NCP) in spring and vertical mixing in autumn [*Hood and Merlivat*, 2001; *Bégovic and Copin-Montégut*, 2002; *Copin-Montégut et al*., 2004]. Temperature is, however, also the primary driver of both the onset of summer stratification and resulting increase in NCP in spring, and the strengthening of vertical mixing in autumn and winter. The drivers of seasonality in pCO_2 are thus similar to those of pH, although we also found a minor impact of variations in TA. The peak-to-peak amplitudes of pH and temperature in this study are in line with earlier work on the 1998–2011 data of the DYFAMED station showing seasonalities in pH (on the seawater scale) and temperature of ~0.10 and ~9°C, respectively [*Marcellin Yao et al*., 2016]. These authors suggest that temperature is the dominant driver of intraannual pH variations, which is largely supported by our analysis. *Copin-Montégut and Bégovic* [2002] presented pH on the total scale (pH_T), TA, and DIC data of the DYFAMED station between 1998 and 2000. However, as their pH_T data are normalized to 25°C (pH_T^{25}), they lack the effect of temperature. The seasonality in pH_T^{25} of 0.015 that they derived was attributed to the same nontemperature drivers, i.e., NCP and vertical mixing, as the seasonality in pCO_2. Contrary to our results, they did not identify a clear seasonality in surface-water TA. The seasonality in DIC these authors estimated (105 $\mu mol\,kg^{-1}$) is similar to the seasonality of ~100 $\mu mol\,kg^{-1}$ determined in more recent studies spanning the 1998–2013 and 1998–2011 periods, respectively [*Gemayel et al*., 2015; *Marcellin Yao et al*., 2016]. All of these values are, however, almost twice as high as the peak-to-peak amplitude of DIC determined in this study. This may be attributed to either the longer timespan of the current data set compared to *Copin-Montégut and Bégovic* [2002], thereby including interannual variability, or to the different methodology this study uses to determine the seasonal mean compared to *Gemayel et al*. [2015] and *Marcellin Yao et al*. [2016].

4.2. Seasonal Variability at Station ALOHA

Seasonal carbonate system variability at Station ALOHA has been extensively studied. *Dore et al*. [2009] presented seasonal variability of pH_T and temperature at Station ALOHA between 1988 and 2007. Their timings of minimum and maximum temperatures (February–March and September, respectively) concur with our harmonic fit (Figure 1e). Moreover, the timing of their pH_T maximum agrees with the pH_{pred} maximum in this study, but their minimum in pH_T was in September, which is later in the year than the minima of pH_{fit} (late August) and pH_{pred} (late July).

Previous studies have shown a seasonality in salinity-normalized DIC (sDIC) at Station ALOHA of 14 $\mu mol\,kg^{-1}$ between 1994 and 1999 [*Quay and Stutsman*, 2003] and of 15 $\mu mol\,kg^{-1}$ between 1998 and 2002 [*Keeling et al*., 2004], consistent with our peak-to-peak amplitude of 13 $\mu mol\,kg^{-1}$ for DIC. The timings of the sDIC extremes found by *Quay and Stutsman* [2003] (April and October–November) and *Keeling et al*. [2004] (early April and October) are in line with the period of minimum and maximum DIC in this study. The data period covered in our study, i.e., 1990–2013, is longer than that of these previous studies and thus includes greater

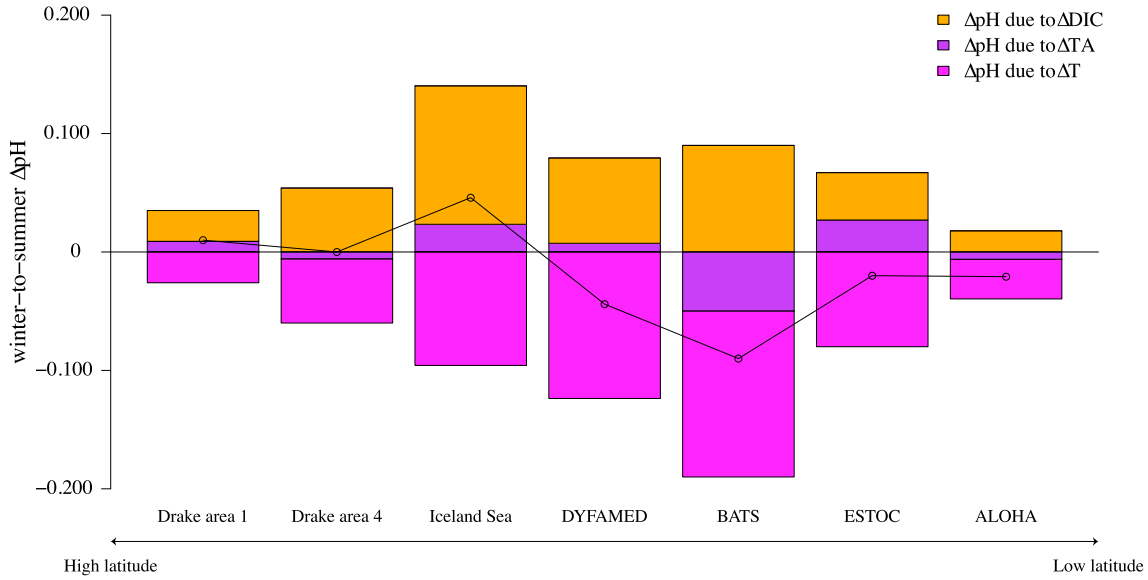

Figure 2. Quantitative contribution of *T*, DIC, and TA changes to winter-to-summer differences in pH. Stations DYFAMED, ALOHA, and Iceland Sea are from this study and stations BATS, ESTOC, and Drake Passage areas 1 and 4 are from *Takahashi et al.* [2014]. The effect of the drivers on pH was calculated by subtracting the average July–September pH from the average January–March pH. For the Drake Passage sites, located on the Southern Hemisphere, the reverse subtraction was made. The dots show the winter-to-summer change of pH_{pred}, which is calculated including the seasonality of factors having a minor effect on pH seasonality, such as salinity.

interannual carbonate system variability due the Pacific Decadal Oscillation and the El Niño–Southern Oscillation [*Winn et al.*, 1994; *Dore et al.*, 2003, 2009; *Brix et al.*, 2004]. This many explain the scatter of both DIC and TA measurements around their respective harmonic fits and may also explain why, using a different methodology, *Takahashi et al.* [2014] could not identify a clear seasonality in both parameters.

Keeling et al. [2004] showed that the seasonal cycle of pCO_2 at station ALOHA is dominated by the temperature-driven pCO_2 changes and modulated by the seasonal DIC variability, which, in turn, is primarily not only governed by NCP but also impacted by horizontal transport and air-sea exchange. Similarly, *Dore et al.* [2009] compared observed pH_T at in situ temperature to pH_T^{25} and found that DIC has a smaller effect on pH_T than temperature and that they have opposing seasonal patterns, consistent with our results for pH_{pred} (Figure 1n). Conversely, *Takahashi et al.* [2014] attributed seasonal variability in pH_T entirely to changes in temperature.

4.3. Seasonal Variability at the Iceland Sea Site

An earlier paper using the Iceland Sea data set until 2006 [*Olafsson et al.*, 2009] focusing on long-term pH_T trends briefly discussed seasonality in pH_T. They found a much smaller interannual variability in winter compared to summer pH_T measurements, which they related to the exact location and timing of the phytoplankton spring bloom. Scatter in summertime pH was also observed in this study (Figure 1l). Previous studies using a subsample of the data set have investigated the Iceland Sea carbonate system seasonality in more detail [*Takahashi et al.*, 1985, 1993]. They showed that surface-water DIC and pCO_2 are lowest in summer and attributed this to high productivity in combination with reduced vertical mixing as a result of strong summer stratification. As productivity is reduced and mixing is strengthened, this leads to high DIC and pCO_2 in winter.

It has also been shown that the seasonalities in DIC and pCO_2 can be best described by a sawtooth rather than by a sinusoidal pattern; the summertime decrease resulting from the phytoplankton spring bloom occurs at a much higher rate than the autumn and winter increase [*Takahashi et al.*, 1985, 1993]. The winter-to-summertime drop in sDIC found by *Takahashi et al.* [1993] was 100–150 $\mu mol\ kg^{-1}$, i.e., somewhat higher than the 84 $\mu mol\ kg^{-1}$ we found for DIC. Several factors might explain this discrepancy. First, we fitted a sinusoidal rather than a sawtooth curve to the data, which may not fully capture the actual trend. Second, our analysis comprises a longer time period and removes the long-term annual trend from the data. The third reason seems, however, most important: a detailed analysis on the late spring/early summer data confirms the importance of the timing of the phytoplankton spring bloom on the interannual variability in DIC. Between years DIC

in the samples taken in the final week of May or the first week of June can vary by as much as 78 μmol kg^{-1}. This interannual variability in timing cannot be accounted for by the harmonic fitting procedure, which takes an average timing in DIC extremes for the entire period and therefore smooths the reproduced trend.

4.4. Latitudinal Trends in Factors Driving Seasonality in pH

For three contrasting oceanic sites we were able to quantitatively predict seasonal pH evolution using only changes in *T*, DIC, and TA and generalized sensitivities of these systems. *Takahashi et al.* [2014] used observed seasonal amplitudes of *T*, *S*, DIC, and TA, averaged over a 3 month period and numerically derived approximations for the sensitivities, to calculate seasonal amplitudes for five sites in the ocean, including Station ALOHA. Despite the differences in methodologies, their results for Station ALOHA are similar to ours, with a seasonality in *T* of 3.2°C (this study: 3.0°C), leading to a seasonal pH_T difference of 0.05 ± 0.01 that is in line with our temperature-driven pH difference of 0.0392 and a lack of a clear seasonal signal in TA and DIC, whereas in this study only 12 month periodicities with small amplitudes were found for both parameters. Moreover, and most importantly, they also found that at all sites *T*, DIC, and TA are the principal drivers of seasonal pH variability. *Omar et al.* [2016] studied seasonal cycles of pH in western Norway fjords and found that the combined effect of *T* and TA changes virtually compensates for the opposing effect of DIC changes on seasonal pH variability. Figure 2 shows the quantitative contributions of changes in *T*, DIC, and TA on pH seasonality for two sites in the Southern Ocean (Drake Passage areas 1 and 4), the Iceland Sea station, DYFAMED, Bermuda Atlantic Time-series Study (BATS), European Station for Time series in the Ocean Canary Islands (ESTOC), and Station ALOHA. It is evident that *T* and DIC are the most important factors governing pH variability and that they have opposing signs, with the consequence that net pH changes are limited. TA contributions are generally small and can lead to either higher or lower pH values in summer. Consequently, it appears that seasonal pH dynamics are primary governed by (1) *T* changes due to seasonal warming and cooling and upwelling and (2) DIC fluctuations related to production and consumption of organic matter or upwelling. Furthermore, at most places changes in TA play a moderating role. Temperature dominates seasonality in low-latitude to midlatitude systems, while high-latitude spring blooms like in the Iceland Sea, Drake Passage area 1 [*Takahashi et al.*, 2014], and in Norwegian fjords [*Omar et al.*, 2016] induce large consumption of DIC with the consequence that pH increases during summer despite warming, consistent with findings by *Riebesell et al.* [2009] for the Labrador Sea.

5. Conclusions and Implications

We show that seasonal pH variability can be accurately reproduced using seasonal DIC, temperature, and TA patterns and pH sensitivity factors. Our work confirms that temperature is the principal driver of seasonality in pH in (sub)tropical waters [*Takahashi et al.*, 2014] but extends this work to a general pattern showing that the winter-to-summer drawdown in DIC becomes increasingly important for seasonal pH variability at higher latitudes. Our approach can be applied to any temporal scale and may therefore be valuable when interpreting high-resolution mooring data at coastal or open ocean sites [*Sutton et al.*, 2016].

With projected global change the relative role of each driver may change. Although marine productivity is projected to decrease over the course of the 21st century globally [*Bopp et al.*, 2013], it may increase locally. Both the magnitude and the timing of the onset of spring blooms may change and thereby impact DIC seasonality. This is mainly due to warming, which enhances cell division rates [*Hunter-Cevera et al.*, 2016] and induces changes in stratification [*Yamada and Ishizaka*, 2006]. Future seasonality in TA will be impacted by intraannual salinity changes resulting from sea-ice melting [*Comiso*, 2010] and intensification of the hydrological cycle [*Levang and Schmitt*, 2015]. However, not only the seasonal cycles of DIC, temperature, and TA are expected to change but also the sensitivity of pH to a perturbation. Future ocean pH will be more sensitive to DIC and TA changes but less impacted by temperature changes [*Hagens and Middelburg*, 2016], possibly resulting in amplified pH seasonality. The combined impact of different seasonal patterns and elevated sensitivities will ultimately determine future seasonal pH variability.

Acknowledgments
This research is supported by the National Ocean and Coastal Research Programme of the Netherlands Organisation for Scientific Research (NWO; grant 83910502) and the Netherlands Earth System Science Centre (NESSC). The DYFAMED time series is funded by CNRS-INSU and ALLENVI through the MOOSE observing network. Part of its data was extracted from the SEANOE landing page (http://www.seanoe.org/data/00326/43749/); additional data were kindly provided by Dr. L. Coppola of the Oceanological Observatory of Villefranche-sur-Mer. The HOT time series data were acquired with funding from the National Science Foundation (NSF) and State of Hawaii general funds and were obtained from the HOT-DOGS platform (http://hahana.soest.hawaii.edu/hot/hot-dogs/interface.html). The Iceland Sea time series data were collected by the Marine Research Institute in Iceland with funding from the European Community Sixth and Seventh Framework Programs and downloaded from the Carbon Dioxide Information Analysis Center (http://cdiac.ornl.gov/oceans/Moorings/Iceland_Sea.html). We thank an anonymous reviewer for constructive feedback that has improved the paper.

References

Bates, D. M., and D. G. Watts (Eds) (1988), *Nonlinear Regression Analysis and Its Applications*, *Wiley Series in Probability and Statistics*, John Wiley, Hoboken, N J.

Bates, N. R., Y. M. Astor, M. J. Church, K. Currie, J. E. Dore, M. González-Dávila, L. Lorenzoni, F. Muller-Karger, J. Olafsson, and J. M. Santana-Casiano (2014), A time-series view of changing ocean chemistry due to ocean uptake of anthropogenic CO_2 and ocean acidification, *Oceanography*, *27*(1), 126–141, doi:10.5670/oceanog.2014.16.

Bégovic, M., and C. Copin-Montégut (2002), Processes controlling annual variations in the partial pressure of CO_2 in surface waters of the central northwestern Mediterranean Sea (DYFAMED site), *Deep Sea Res. Part II Top. Stud. Oceanogr.*, *49*(11), 2031–2047, doi:10.1016/S0967-0645(02)00026-7.

Bopp, L., et al. (2013), Multiple stressors of ocean ecosystems in the 21st century: Projections with CMIP5 models, *Biogeosciences*, *10*(10), 6225–6245, doi:10.5194/bg-10-6225-2013.

Brix, H., N. Gruber, and C. D. Keeling (2004), Interannual variability of the upper ocean carbon cycle at station ALOHA near Hawaii, *Global Biogeochem. Cycles*, *18*, GB4019, doi:10.1029/2004GB002245.

Comiso, J. (2010), *Polar Oceans From Space*, *Atmospheric and Oceanographic Sciences Library*, Springer, New York.

Copin-Montégut, C., and M. Bégovic (2002), Distributions of carbonate properties and oxygen along the water column (0–2000 m) in the central part of the NW Mediterranean Sea (DYFAMED site): Influence of winter vertical mixing on air–sea CO_2 and O_2 exchanges, *Deep Sea Res. Part II Top. Stud. Oceanogr.*, *49*(11), 2049–2066, doi:10.1016/S0967-0645(02)00027-9.

Copin-Montégut, C., M. Bégovic, and L. Merlivat (2004), Variability of the partial pressure of CO_2 on diel to annual time scales in the northwestern Mediterranean Sea, *Mar. Chem.*, *85*(3–4), 169–189, doi:10.1016/j.marchem.2003.10.005.

Coppola, L., E. Diamond Riquier, and T. Carval (2016), DYFAMED observatory data, *SEANOE*, doi:10.17882/43749.

Dickson, A. G. (1981), An exact definition of total alkalinity and a procedure for the estimation of alkalinity and total inorganic carbon from titration data, *Deep Sea Res. Part A. Oceanogr. Res. Pap.*, *28*(6), 609–623, doi:10.1016/0198-0149(81)90121-7.

Dickson, A. G., C. L. Sabine, and J. R. Christian (Eds.) (2007), *Guide to Best Practices for Ocean CO_2 Measurements*, *PICES Spec. Publ.*, vol. 3, North Pacific Marine Science Organization, Sidney, Canada.

Dore, J. E., R. Lukas, D. W. Sadler, and D. M. Karl (2003), Climate-driven changes to the atmospheric CO_2 sink in the subtropical North Pacific Ocean, *Nature*, *424*(6950), 754–757, doi:10.1038/nature01885.

Dore, J. E., R. Lukas, D. W. Sadler, M. J. Church, and D. M. Karl (2009), Physical and biogeochemical modulation of ocean acidification in the central North Pacific, *Proc. Natl. Acad. Sci. U.S.A.*, *106*(30), 12,235–12,240, doi:10.1073/pnas.0906044106.

Egleston, E. S., C. L. Sabine, and F. M. M. Morel (2010), Revelle revisited: Buffer factors that quantify the response of ocean chemistry to changes in DIC and alkalinity, *Global Biogeochem. Cycles*, *24*, GB1002, doi:10.1029/2008GB003407.

Fabry, V., J. McClintock, J. Mathis, and J. Grebmeier (2009), Ocean acidification at high latitudes: The bellwether, *Oceanography*, *22*(4), 160–171, doi:10.5670/oceanog.2009.105.

Flecha, S., F. F. Pérez, J. García-Lafuente, S. Sammartino, A. F. Ríos, and I. E. Huertas (2015), Trends of pH decrease in the Mediterranean Sea through high frequency observational data: Indication of ocean acidification in the basin, *Sci. Rep.*, *5*, 16,770, doi:10.1038/srep16770.

Frankignoulle, M. (1994), A complete set of buffer factors for acid/base CO_2 system in seawater, *J. Mar. Syst.*, *5*(2), 111–118, doi:10.1016/0924-7963(94)90026-4.

Gattuso, J.-P., L. Hansson, and F. Gazeau (2014), Ocean acidification and its consequences, in *Ocean in the Earth System*, edited by A. Monaco and P. Prouzet, pp. 189–253, John Wiley, Hoboken, N. J.

Gemayel, E., A. E. R. Hassoun, M. A. Benallal, C. Goyet, P. Rivaro, M. Abboud-Abi Saab, E. Krasakopoulou, F. Touratier, and P. Ziveri (2015), Climatological variations of total alkalinity and total dissolved inorganic carbon in the Mediterranean Sea surface waters, *Earth Syst. Dyn.*, *6*(2), 789–800, doi:10.5194/esd-6-789-2015.

Gruber, N., C. D. Keeling, and T. F. Stocker (1998), Carbon-13 constraints on the seasonal inorganic carbon budget at the BATS site in the northwestern Sargasso Sea, *Deep Sea Res. Part I Oceanogr. Res. Pap.*, *45*(4–5), 673–717, doi:10.1016/S0967-0637(97)00098-8.

Gruber, N., C. D. Keeling, and N. R. Bates (2002), Interannual variability in the North Atlantic Ocean carbon sink, *Science*, *298*(5602), 2374–2378, doi:10.1126/science.1077077.

Hagens, M., and J. J. Middelburg (2016), Generalised expressions for the response of pH to changes in ocean chemistry, *Geochim. Cosmochim. Acta*, *187*, 334–349, doi:10.1016/j.gca.2016.04.012.

Hofmann, A. F., J. J. Middelburg, K. Soetaert, and F. J. R. Meysman (2009), pH modelling in aquatic systems with time-variable acid-base dissociation constants applied to the turbid, tidal Scheldt estuary, *Biogeosciences*, *6*(8), 1539–1561, doi:10.5194/bg-6-1539-2009.

Hofmann, A. F., K. Soetaert, J. J. Middelburg, and F. J. R. Meysman (2010), AquaEnv: An aquatic acid–base modelling environment in R, *Aquat. Geochem.*, *16*(4), 507–546, doi:10.1007/s10498-009-9084-1.

Hofmann, G. E., et al. (2011), High-frequency dynamics of ocean pH: A multi-ecosystem comparison, *PLoS One*, *6*(12, e28983), doi:10.1371/journal.pone.0028983.

Hood, E. M., and L. Merlivat (2001), Annual to interannual variations of fCO_2 in the northwestern Mediterranean Sea: Results from hourly measurements made by CARIOCA buoys, 1995-1997, *J. Mar. Res.*, *59*(1), 113–131, doi:10.1357/002224001321237399.

Hunter-Cevera, K. R., M. G. Neubert, R. J. Olson, A. R. Solow, A. Shalapyonok, and H. M. Sosik (2016), Physiological and ecological drivers of early spring blooms of a coastal phytoplankter, *Science*, *354*(6310), 326–329, doi:10.1126/science.aaf8536.

Kapsenberg, L., and G. E. Hofmann (2016), Ocean pH time-series and drivers of variability along the northern Channel Islands, California, USA, *Limnol. Oceanogr.*, *61*(3), 953–968, doi:10.1002/lno.10264.

Keeling, C. D. (1993), Lecture 2: Surface ocean CO_2, in *The Global Carbon Cycle*, *NATO ASI Ser.*, vol. 15, edited by M. Heimann, pp. 413–429, Springer, Berlin.

Keeling, C. D., H. Brix, and N. Gruber (2004), Seasonal and long-term dynamics of the upper ocean carbon cycle at Station ALOHA near Hawaii, *Global Biogeochem. Cycles*, *18*, GB4006, doi:10.1029/2004GB002227.

Kleypas, J. A., R. W. Buddemeier, D. Archer, J.-P. Gattuso, C. Langdon, and B. N. Opdyke (1999), Geochemical consequences of increased atmospheric carbon dioxide on coral reefs, *Science*, *284*(5411), 118–120, doi:10.1126/science.284.5411.118.

Lauvset, S. K., N. Gruber, P. Landschützer, A. Olsen, and J. Tjiputra (2015), Trends and drivers in global surface ocean pH over the past 3 decades, *Biogeosciences*, *12*(5), 1285–1298, doi:10.5194/bg-12-1285-2015.

Levang, S. J., and R. W. Schmitt (2015), Centennial changes of the global water cycle in CMIP5 models, *J. Clim.*, *28*(16), 6489–6502, doi:10.1175/JCLI-D-15-0143.1.

Lueker, T. J., A. G. Dickson, and C. D. Keeling (2000), Ocean pCO_2 calculated from dissolved inorganic carbon, alkalinity, and equations for K_1 and K_2: Validation based on laboratory measurements of CO_2 in gas and seawater at equilibrium, *Mar. Chem.*, *70*(1–3), 105–119, doi:10.1016/S0304-4203(00)00022-0.

Marcellin Yao, K., O. Marcou, C. Goyet, V. Guglielmi, F. Touratier, and J.-P. Savy (2016), Time variability of the north-western Mediterranean Sea pH over 1995–2011, *Mar. Environ. Res.*, *116*, 51–60, doi:10.1016/j.marenvres.2016.02.016.

Olafsson, J. (2014), Iceland Sea time series data from the 1985–2013 cruises, *Carbon Dioxide Inf. Anal. Center*, *Oak Ridge Natl. Lab. U.S. Dep. Energy*, *Oak Ridge*, *Tennessee*, doi:10.3334/CDIAC/otg.CARINA_IcelandSea_V2.

Olafsson, J., S. R. Ólafsdóttir, A. Benoit-Cattin, M. Danielsen, T. S. Arnarson, and T. Takahashi (2009), Rate of Iceland Sea acidification from time series measurements, *Biogeosciences*, *6*(11), 2661–2668, doi:10.5194/bg-6-2661-2009.

Olafsson, J., S. R. Ólafsdóttir, A. Benoit-Cattin, and T. Takahashi (2010), The Irminger Sea and the Iceland Sea time series measurements of sea water carbon and nutrient chemistry 1983–2008, *Earth Syst. Sci. Data*, *2*(1), 99–104, doi:10.5194/essd-2-99-2010.

Omar, A. M., I. Skjelvan, S. R. Erga, and A. Olsen (2016), Aragonite saturation states and pH in western Norwegian fjords: Seasonal cycles and controlling factors, 2005–2009, *Ocean Sci.*, *12*(4), 937–951, doi:10.5194/os-12-937-2016.

Orr, J. C. (2011), Recent and future changes in ocean carbonate chemistry, in *Ocean Acidification*, edited by J.-P. Gattuso and L. Hansson, pp. 41–66, Oxford Univ. Press, Oxford.

Pasqueron de Fommervault, O., C. Migon, F. D'Ortenzio, M. Ribera d'Alcalà, and L. Coppola (2015), Temporal variability of nutrient concentrations in the northwestern Mediterranean sea (DYFAMED time-series station), *Deep Sea Res. Part I Oceanogr. Res. Pap.*, *100*, 1–12, doi:10.1016/j.dsr.2015.02.006.

Provoost, P., S. van Heuven, K. Soetaert, R. W. P. M. Laane, and J. J. Middelburg (2010), Seasonal and long-term changes in pH in the Dutch coastal zone, *Biogeosciences*, *7*(11), 3869–3878, doi:10.5194/bg-7-3869-2010.

Quay, P., and J. Stutsman (2003), Surface layer carbon budget for the subtropical N. Pacific: Constraints at station ALOHA, *Deep Sea Res. Part I Oceanogr. Res. Pap.*, *50*(9), 1045–1061, doi:10.1016/S0967-0637(03)00116-X.

R Core Team (2016), R: A language and environment for statistical computing.

Riebesell, U., A. Körtzinger, and A. Oschlies (2009), Sensitivities of marine carbon fluxes to ocean change, *Proc. Natl. Acad. Sci. U.S.A.*, *106*(49), 20,602–20,609, doi:10.1073/pnas.0813291106.

Ríos, A. F., L. Resplandy, M. I. García-Ibáñez, N. M. Fajar, A. Velo, X. A. Padin, R. Wanninkhof, R. Steinfeldt, G. Rosón, and F. F. Pérez (2015), Decadal acidification in the water masses of the Atlantic Ocean, *Proc. Natl. Acad. Sci. U.S.A.*, *112*(32), 9950–9955, doi:10.1073/pnas.1504613112.

Sarmiento, J. L., and N. Gruber (2006), *Ocean Biogeochemical Dynamics*, Princeton Univ. Press, Princeton, N. J.

Shadwick, E. H., H. Thomas, K. Azetsu-Scott, B. J. W. Greenan, E. Head, and E. Horne (2011), Seasonal variability of dissolved inorganic carbon and surface water pCO_2 in the Scotian Shelf region of the Northwestern Atlantic, *Mar. Chem.*, *124*(1–4), 23–37, doi:10.1016/j.marchem.2010.11.004.

Shadwick, E. H., T. W. Trull, H. Thomas, and J. A. E. Gibson (2013), Vulnerability of polar oceans to anthropogenic acidification: Comparison of Arctic and Antarctic seasonal cycles, *Sci. Rep.*, *3*, 2339, doi:10.1038/srep02339.

Soetaert, K., A. F. Hofmann, J. J. Middelburg, F. J. R. Meysman, and J. Greenwood (2007), The effect of biogeochemical processes on pH, *Mar. Chem.*, *105*(1–2), 30–51, doi:10.1016/j.marchem.2006.12.012.

Sutton, A. J., et al. (2016), Using present-day observations to detect when anthropogenic change forces surface ocean carbonate chemistry outside preindustrial bounds, *Biogeosciences*, *13*(17), 5065–5083, doi:10.5194/bg-13-5065-2016.

Takahashi, T., J. Olafsson, W. S. Broecker, J. G. Goddard, D. W. Chipman, and J. White (1985), Seasonal variability of the carbon-nutrient chemistry in the ocean areas west and north of Iceland, *Rit Fiskid.*, *9*, 20–36.

Takahashi, T., J. Olafsson, J. G. Goddard, D. W. Chipman, and S. C. Sutherland (1993), Seasonal variation of CO_2 and nutrients in the high-latitude surface oceans: A comparative study, *Global Biogeochem. Cycles*, *7*(4), 843–878, doi:10.1029/93GB02263.

Takahashi, T., et al. (2002), Global sea–air CO_2 flux based on climatological surface ocean pCO_2, and seasonal biological and temperature effects, *Deep Sea Res. Part II Top. Stud. Oceanogr.*, *49*(9–10), 1601–1622, doi:10.1016/S0967-0645(02)00003-6.

Takahashi, T., S. C. Sutherland, D. W. Chipman, J. G. Goddard, C. Ho, T. Newberger, C. Sweeney, and D. R. Munro (2014), Climatological distributions of pH, pCO_2, total CO_2, alkalinity, and $CaCO_3$ saturation in the global surface ocean, and temporal changes at selected locations, *Mar. Chem.*, *164*, 95–125, doi:10.1016/j.marchem.2014.06.004.

Winn, C. D., F. T. Mackenzie, C. J. Carrillo, C. L. Sabine, and D. M. Karl (1994), Air-sea carbon dioxide exchange in the North Pacific Subtropical Gyre: Implications for the global carbon budget, *Global Biogeochem. Cycles*, *8*(2), 157–163, doi:10.1029/94GB00387.

Wootton, J. T., and C. A. Pfister (2012), Carbon system measurements and potential climatic drivers at a site of rapidly declining ocean pH, *PLoS One*, *7*(12, e53396), doi:10.1371/journal.pone.0053396.

Wootton, J. T., C. A. Pfister, and J. D. Forester (2008), Dynamic patterns and ecological impacts of declining ocean pH in a high-resolution multi-year dataset, *Proc. Natl. Acad. Sci. U.S.A.*, *105*(48), 18,848–18,853, doi:10.1073/pnas.0810079105.

Yamada, K., and J. Ishizaka (2006), Estimation of interdecadal change of spring bloom timing, in the case of the Japan Sea, *Geophys. Res. Lett.*, *33*, L02608, doi:10.1029/2005GL024792.